exceeds that previously reported.

The performance of the SCMCR could be improved by using a different catalyst and adsorbent combination. Promoted catalysts (*16*, *17*) and hydrothermally treated lanthanide oxides (*18*) with somewhat better activity and selectivity than unpromoted Sm_2O_3 have been reported. Furthermore, a limitation of the CH_4 conversion in these experiments is the loss of CH_4 from the adsorption columns. The charcoal adsorbent has a heterogeneous surface on which some of the CH_4 is relatively strongly adsorbed, enough so that a portion is not carried forward to undergo further reaction but remains behind as the feed section is advanced. It is then purged away by the carrier gas just before the section in which it resides becomes the feed section once more. Greater CH_4 conversions and higher C_2 yields would be obtained if the CH_4 loss were eliminated. This could be accomplished by using an adsorbent on which CH_4 tailing is reduced, and if necessary by increasing the number of reactor-adsorber sections.

The performance might also be enhanced by working at lower CH_4/O_2 ratios. Microreactor studies showed that at 725°C, the C_2 selectivity only decreased from 97% at $CH_4/O_2 = 50$ to 95% at $CH_4/O_2 = 20$. At smaller ratios, the conversion per pass is expected to be larger, so the C_2 yield in the SCMCR is expected to increase. This effect would be offset somewhat by oxidation of the C_2s.

REFERENCES AND NOTES

1. G. E. Keller and M. M. Bhasin, *J. Catal.* **73**, 9 (1982).
2. W. Hinsen and M. Baerns, *Chem.-Zlit.* **107**, 223 (1983).
3. T. Ito and J. H. Lunsford, *Nature* **314**, 721 (1985).
4. U. Preuss and M. Baerns, *Chem. Eng. Technol.* **10**, 297 (1987).
5. J. R. Anderson, *Appl. Catal.* **47**, 177 (1989).
6. J. S. Lee and S. T. Oyama, *Catal. Rev.-Sci. Eng.* **30**, 249 (1988).
7. G. J. Hutchings, M. S. Scurrell, J. R. Woodhouse, *Chem. Soc. Rev.* **18**, 251 (1989).
8. J. H. Lunsford, *Catal. Today* **6**, 235 (1991).
9. A. Ray, A. L. Tonkovich, R. Aris, R. W. Carr, *Chem. Eng. Sci.* **45**, 2431 (1990).
10. S. H. Langer, J. Y. Yurchak, J. E. Patton, *Ind. Eng. Chem.* **61**, 11 (1969).
11. B. K. Cho, R. W. Carr, R. Aris, *Chem. Eng. Sci.* **35**, 74 (1980).
12. B. B. Fish and R. W. Carr, *ibid.* **44**, 1773 (1989).
13. K. Otsuka, K. Jinno, A. Morikawa, *Chem. Lett.* **1985**, 499 (1985); *J. Catal.* **100**, 353 (1986).
14. B. B. Fish, R. W. Carr, R. Aris, *Chem. Eng. Sci.* **43**, 1867 (1988).
15. O. Levenspiel, *Chemical Reaction Engineering* (Wiley, New York, ed. 2, 1972), pp. 144–149.
16. K. Otsuka, Q. Liu, M. Hatano, A. Morikawa, *Chem. Lett.* **1986**, 467 (1986).
17. G. J. Hutchings, J. R. Woodhouse, M. S. Scurrell, *J. Chem. Soc. Faraday Trans I* **85**, 2507 (1989).
18. K. D. Campbell, H. Zhang, J. H. Lunsford, *J. Phys. Chem.* **92**, 750 (1988).
19. Supported by the Division of Chemical Sciences, Office of Basic Energy Sciences, U.S. Department of Energy, under grant number DE-AC02-76-ER02945.

6 April 1993; accepted 29 July 1993

Molecular Dynamics Simulations of a Lipid Bilayer and of Hexadecane: An Investigation of Membrane Fluidity

Richard M. Venable, Yuhong Zhang, Barry J. Hardy, Richard W. Pastor*

Molecular dynamics simulations of a fluid-phase dipalmitoyl phosphatidylcholine lipid bilayer in water and of neat hexadecane are reported and compared with nuclear magnetic resonance spin-lattice relaxation and quasi-elastic neutron scattering data. On the 100-picosecond time scale of the present simulations, there is effectively no difference in the reorientational dynamics of the carbons in the membrane interior and in pure hexadecane. Given that the calculated fast reorientational correlation times and the "microscopic" lateral diffusion of the lipids show excellent agreement with the experimental results, it is concluded that the apparently high viscosity of the membrane is more closely related to molecular interactions on the surface rather than in the interior.

Lipid membranes show an almost paradoxical combination of fluidity and rigidity. As noted by Overton (*1*) almost a century ago and by many others since then (*2*), the membrane behaves very much like an oil drop in terms of the solubility and diffusion of small nonpolar molecules. In contrast, the translational diffusion constants of lipids and proteins in membranes are characteristic of media with viscosity over two orders of magnitude higher than that of an oil such as hexadecane (*3*). An understanding of the molecular basis of this behavior is essential for elucidating transport phenomena in membranes. For example, when quinone crosses the bilayer in the oxidation-reduction pathway, is it diffusing in a low- or high-viscosity fluid? To begin to provide the molecular details of diffusion in membranes, we report the results of molecular dynamics (MD) simulations of a dipalmitoyl phosphatidylcholine (DPPC) lipid bilayer in water and of neat hexadecane; both simulations were carried out at the same temperature (50°C) with the use of identical potential energy parameters (*4*), thus enabling straightforward comparisons.

MD studies of monolayers (*5*), bilayers (*6*, *7*), and micelles (*8*) interacting with solvent are relatively recent. This is due in part to the fact that membranes are lyotropic, and the stability of the simulation is sensitive to details of the potential energy parametrization (*5*, *6*). Additionally, and in contrast to the case for proteins and DNA where x-ray structures provide reasonable initial conditions for a simulation (*9*), the biologically active (L_α) phase of lipid bilayers is disordered and information from the crystal (L_c) or gel (L_β) phases is not directly relevant (*10*, *11*). Here initial conditions for the L_α phase bilayer were developed using a mean field approach. In our two-step method, we first generated conformations of individual lipids in a Marcelja mean field (*12*), using a recently developed torsional Monte Carlo procedure (*13*); the parameters of the field were adjusted so that the average orientations were consistent with experimental deuterium order parameters (S_{CD}) (*14*). Second, 72 independent configurations were packed into an L_α phase bilayer-water assembly with appropriate dimensions (*15*). This procedure circumvents the long equilibration time otherwise necessary to obtain a configuration consistent with experimental order parameters and dimensions when starting with more gel-like distributions [for additional details, see (*16*, *17*)].

Figure 1 shows an 8 Å slab from the system at 120 ps (approximately midway through the simulation). The liquid-like nature of the bilayer interior and the solvation of the headgroup and glycerol region are evident. The movement of a selected set of eight lipids (part of one row) over the interval 100 to 190 ps is illustrated in Fig. 2. It is clear that on this time scale the chain dynamics consist primarily of dihedral angle isomerization and other local motions, with little overall rotation or translation of the lipids. We first compare these short-time reorientations with those of hexadecane and with experiment and then proceed to the consideration of molecular translation.

The simulated reorientational correlation functions,

$$\langle P_2[\hat{\mu}(t) \cdot \hat{\mu}(0)]\rangle = \langle \tfrac{3}{2} [\hat{\mu}(t) \cdot \mu(0)]^2 - \tfrac{1}{2}\rangle$$

where P_2 is the second rank Legendre polynomial, $\hat{\mu}$ is a unit vector, and t is time, are shown in Fig. 3 for selected CH vectors of

---

Biophysics Laboratory, Center for Biologics Evaluation and Research, Food and Drug Administration, 8800 Rockville Pike, Bethesda, MD 20892.

*To whom correspondence should be addressed.

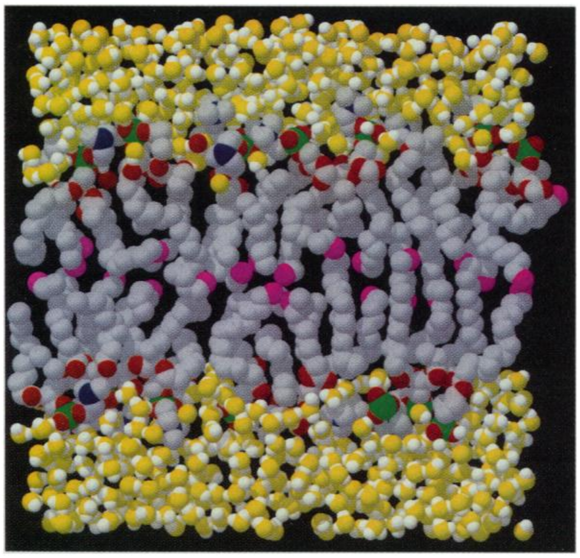

Fig. 1. An 8 Å slab from the system, taken along one of the diagonals, after 120 ps of MD simulation. The coloring is as follows: phosphorus, green; nitrogen, dark blue; lipid oxygens, red; terminal chain methyl groups, magenta; other carbons, gray; water oxygens, yellow; and water hydrogens, white. For clarity, the radii of heavy atoms are reduced slightly from their van der Waals values, radii of water hydrogens are increased, and carbon hydrogens are omitted.

the bilayer chains and for hexadecane. The lipid correlation functions are known experimentally to consist of fast ($\tau_f < 250$ ps) and slow ($\tau_s \approx$ nanosecond and longer) components (*18–21*), although their physical origin has been debated. We make three essential points regarding these data. First, as shown in Table 1, the simulated τ_f values for the bilayer chain carbons are in excellent agreement with those derived from experiment. From inspection of Fig. 2, we infer that most of the fast relaxation arises from isomerizations; these rates are shown in Fig. 4. Second, the simulated correlation functions, τ_f, and isomerization rates obtained for hexadecane show a remarkable correspondence to those found for the bilayer chains on a carbon-by-carbon basis (see Figs. 3 and 4 and Table 1). Hence, at least on the 100-ps time scale for local motions, the effective viscosity of the bilayer interior is very similar to that of a neat alkane of approximately the same chain length; this assertion was made by Brown *et al.* (*21*) on the basis of nuclear magnetic resonance (NMR) relaxation studies and later by Pastor *et al.* (*19*) from an analysis of Brownian dynamics simulations. Third, even though the isomerization rates are well converged, none of the lipid correlation functions have reached their plateau values on the time scale of the simulation (Table 1 and Fig. 3). This feature is consistent with both stochastic dynamics simulations (*18*, *19*) and NMR studies (*20*, *21*), where it was shown that the reorientation, or "wobble," of the long axis of the lipids takes place on the nanosecond time scale.

To study molecular translation, we evaluated the root-mean-square (rms) displacements of the center of mass as a function of time; the diffusion constant is proportional to the long-time slope of this function. The simulated diffusion constant for hexadecane, 5.7×10^{-6} cm^2/s, is in good agreement with the value interpolated from experiment, 6.7×10^{-6} cm^2/s (*22*). Experimental lateral diffusion constants for lipids and related probe molecules fall in the range 10^{-7} to 10^{-8} cm^2/s at 50°C (*3*, *10*, *11*, *23*), and hence the self-diffusion constant of DPPC is too small to quantify here. Our data, however, are consistent with experimental results in that no two lipids exchanged places (see Fig. 5). Furthermore, the short-time slope of the lateral displacements versus time (evaluated from 1 to 10 ps) yielded a "microscopic" diffusion constant of 2×10^{-6} cm^2/s, in reasonable agreement with the value 4×10^{-6} cm^2/s obtained for DPPC bilayers at 63°C from quasi-elastic neutron scattering (*24*). This rapid component of translation clearly evident in Fig. 5 has been denoted "rattle" (*23*), to describe the oscillation of the lipid within the cage of its nearest neighbors. The present simulation indicates that rattle is diffusive (rather than inertial) and results in part from coupling of the center-of-mass translation with isomerizations.

As will be described in more detail elsewhere (*25*), the average conformations of the individual hexadecane and DPPC chains are also similar. For example, the simulated rms end-to-end distance is 14.5 Å for hexadecane, which corresponds to a persistence length of 10.5 Å and indicates that the chains are, on average, relatively extended. The rms distance between carbons 1 and 16 for the bilayer was 14.7 Å. This does not imply, however, that the interchain structures of the bilayer interior and hexadecane are identical. On average, the membrane chains are oriented along the bilayer normal and their individual carbons are more localized than in the simulated hexadecane. There is, interestingly, experimental evidence that liquid alkanes also contain regions of relatively high local order (*26*).

The striking similarities of the short-time dynamics and conformations of the lipid chains and neat hexadecane shown here are consistent with the essential features of the

Table 1. Fast correlation times and fitting parameters. Simulated correlation functions for bilayer CH vectors were fit, over their first 50 ps, with the function:

$$\sum_{i=1}^{3} a_i \exp(-t/\tau_i) + A_s^2 \exp(-t/\tau_s) + S_{CD}^2$$

The fast correlation time is given by

$$\tau_f^{sim} = \left(\sum_{i=1}^{3} a_i \tau_i\right) \Bigg/ \left(\sum_{i=1}^{3} a_i\right)$$

Values for experimental fast (τ_f^{exp}) and slow relaxation times ($\tau_s = 1.83$ ns) and amplitudes (A_s^2) were obtained from a two-exponential fit to the frequency-dependent spin-lattice relaxation time data of Brown and co-workers (*21*), as described in (*19*); $(S_{CD}^2)^{exp}$ is the average squared experimental deuterium order parameter (*14*) for each carbon or set of carbons. The statistical error in the correlation functions is small over the interval shown (<7%) because the average is taken over all chains. The derived fitted values of τ_f increase from 3 to 7% if $(S_{CD}^2)^{sim}$ values are used in the analysis. Simulated $|S_{CD}|$ values are, on average, 20% below experimental values; however, as discussed elsewhere (*16*), their statistical uncertainty is very high because time-averaging over the slow motions is incomplete. Hexadecane correlation functions were fit with three exponentials with no added plateau value or slow correlation time, and τ_f^{sim} was calculated as for the bilayer.

Carbon	Lipid bilayer					Hexadecane
	τ_f^{sim} (ps)	τ_f^{exp} (ps)	A_s^2	$(S_{CD}^2)^{exp}$	$(S_{CD}^2)^{sim}$	τ_f^{sim} (ps)
2	48	41.4	0.0615	0.0305	0.022	
3	43	32.3	0.0396	0.0374	0.028	
4–13	23	20.4	0.0355	0.0350	0.023	17.2 (C-8 and C-9)
14	8.5	9.5	0.0231	0.0123	0.0046	8.7 (C-3 and C-14)
15	6.8	6.8	0.00989	0.00667	0.0034	6.5 (C-2 and C-15)

Fig. 2. An overlay of 10 frames, 10 ps apart over the interval 100 to 190 ps of a selected set of eight lipids. A comparison of this figure and figure 3c of (*18*) (where 10-ps intervals are plotted from a Langevin simulation of DPPC) reveals very similar dynamics.

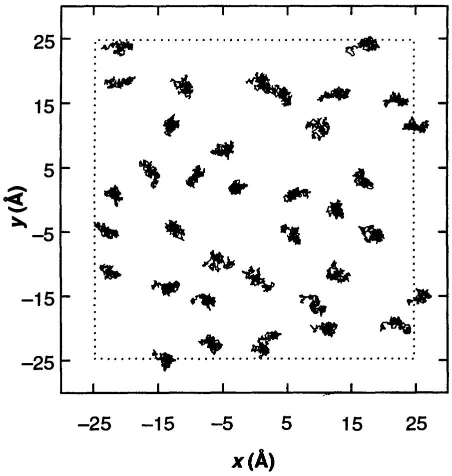

Fig. 5. Trajectories over the interval 20 to 190 ps showing lateral diffusion of the centers of mass of the lipids comprising the top half of the bilayer. Dotted lines show the boundaries of the periodic box.

"oil drop model" (*1, 2*). Although our study only indirectly addresses the longer time scale of translational diffusion, the results indicate that the viscosity required to fit experimental data based on the use of hydrodynamic (*3*) and elastic theories (*27*) of membranes (typically 100 to 200 centipoise) is not related to the inferred microscopic viscosity of the bilayer interior (~2 centipoise). It is therefore reasonable to conclude that interactions involving the glycerol, headgroup, and surface water principally modulate translational diffusion and that analytic theories should explicitly take into account the dynamic and structural features of the lipid-water interface.

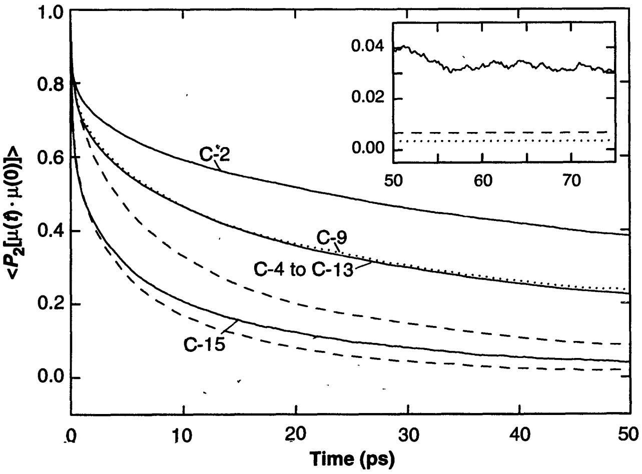

Fig. 3. Reorientational correlation functions for selected CH unit vectors of chain methylene groups in the lipid bilayer and hexadecane. Solid and dotted lines are for the bilayer (C-2 represents the methylene group closest to the carbonyl, C-4 to C-13 is the average of C-4 through C-13, C-15 is adjacent to the terminal methyl). Dashed lines represent hexadecane (the upper line is an average of C-8 and C-9, and the lower line is an average of C-2 and C-15). The inset shows the decay of C-15 from the bilayer on an expanded scale, where the dashed and dotted lines are the experimental and simulated averages of S^2_{CD}, respectively.

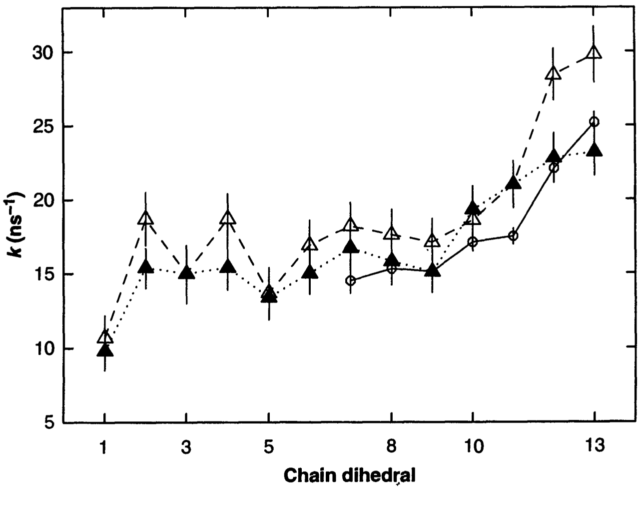

Fig. 4. Isomerization rates for lipid chain and hexadecane torsions. Open triangles represent chain 1 of the bilayer, filled triangles chain 2, and open circles hexadecane (the average rate of hexadecane torsions 1 and 13 is plotted as position 13, 2 and 12 as 12, . . .). We calculated the rates by counting the total number of isomerizations (as defined by a passage over a barrier into the neighboring well) and dividing by the simulation time. Error bars were obtained as the standard deviation of the mean divided by the square root of the number of torsions (that is, 72 for the bilayer and 128 for hexadecane).

REFERENCES AND NOTES

1. E. Overton, *Vierteljahresschr. Naturforsch. Ges. Zurich* **40**, 159 (1895).
2. A. Finkelstein, *Water Movement Through Lipid Bilayers, Pores, and Plasma Membranes: Theory and Reality* (Wiley-Interscience, New York, 1987).
3. P. G. Saffman and M. Delbruck, *Proc. Natl. Acad. Sci. U.S.A.* **72**, 3111 (1975); B. D. Hughes, B. A. Pailthorpe, L. R. White, W. H. Sawyer, *Biophys. J.* **37**, 673 (1982); R. Peters and R. J. Cherry, *Proc. Natl. Acad. Sci. U.S.A.* **79**, 4317 (1982).
4. Parameter set PARM 22 of CHARMM (Chemistry at Harvard Macromolecular Mechanics).
5. P. S. Charifson, R. G. Hiskey, L. G. Pedersen, *J. Comput. Chem.* **10**, 1182 (1990); M. L. Klein, *J. Chem. Soc. Faraday Trans.* **88**, 1701 (1992); P. Ahlström and H. J. C. Berendsen, *J. Phys. Chem.*, in press.
6. B. Egberts, thesis, Rijksuniversiteit Groningen, Groningen (1988); T. R. Stouch, K. B. Ward, A. Altieri, A. Hagler, *J. Comput. Chem.* **12**, 1033 (1991).
7. B. Egberts, W. F. van Gunsteren, H. J. C. Berendsen, *J. Chem. Phys.* **89**, 3718 (1988); K. Raghavan, M. R. Reddy, M. L. Berkowitz, *Langmuir* **8**, 233 (1992); K. V. Damodaran, K. M. Merz, B. P. Gaber, *Biochemistry* **31**, 7656 (1992); T. R. Stouch, *Mol. Simulations* **10**, 317 (1993); H. Heller, M. Schaefer, K. Schulten, *J. Phys. Chem.* **97** 8343 (1993).
8. K. Watanabe and M. L. Klein, *J. Phys. Chem.* **93**, 6897 (1989); B. Jönsson, O. Edholm, O. Teleman, *J. Chem. Phys.* **85**, 2259 (1986); J. J. Wendoloski, S. J. Kimatian, C. E. Schutt, F. R. Salemme, *Science* **243**, 636 (1989).
9. C. L. Brooks, B. M. Pettitt, M. Karplus, *Proteins: A Theoretical Perspective of Dynamics, Structure, and Thermodynamics* (Wiley-Interscience, New York, 1988).
10. D. M. Small, *The Physical Chemistry of Lipids* (Plenum, New York, 1986).
11. G. Cevc and D. Marsh, *Phospholipid Bilayers* (Wiley-Interscience, New York, 1987).
12. S. Marcelja, *Biochim. Biophys. Acta* **367**, 165 (1974); H. Schindler and J. Seelig, *Biochemistry*

14, 2283 (1975); R. W. Pastor, R. M. Venable, M. Karplus, *J. Chem. Phys.* **89**, 1112 (1988); R. W. Pastor, R. M. Venable, M. Karplus, *Proc. Natl. Acad. Sci. U.S.A.* **88**, 892 (1991).

13. B. J. Hardy and R. W. Pastor, *J. Comput. Chem.*, in press.
14. A. Seelig and J. Seelig, *Biochemistry* **13**, 4839 (1974).
15. R. P. Rand and V. A. Parsegian, *Biochim. Biophys. Acta* **998**, 351 (1989).
16. R. W. Pastor and R. M. Venable, in *Computer Simulation of Biomolecular Systems: Theoretical and Experimental Applications*, W. F. van Gunsteren, P. K. Weiner, A. K. Wilkinson, Eds. (ESCOM Science Publishers, Leiden, in press).
17. The membrane system contained 72 lipid molecules and 2533 water molecules for a total of 16,893 atoms (including hydrogens). Dimensions imposed for three-dimensional periodic conditions were consistent with the experimental density (1.0 g/cm^3) and surface area per lipid (68.1 Å^2) for a lipid/water weight ratio of 0.6 (*15*). Lipid phosphorus atoms were placed in a two-dimensional hexagonal array (36 per layer), and a series of energy minimizations eliminated any unphysically close contacts during packing (*16*). We carried out the MD simulation (with no constraints on any atom) for 190 ps (20 ps for heating and equilibration, 170 ps for analysis) at 50°C, constant particle number, volume, and energy with a time step of 0.001 ps using CHARMM [B. R. Brooks *et al., J. Comput. Chem.* **4**, 187 (1983)]; approximately 15 central processor unit (cpu) hours on an IBM 3090 were required for each picosecond of simulation. The hexadecane simulation consisted of 64 molecules at a density of 0.866 g/cm^3. We developed the initial configuration by randomly packing and then energy-minimizing single chains that had been generated by Monte Carlo procedures (*13*). We carried out the simulation for 530 ps on a Hewlett Packard 730 workstation (30 ps for equilibration and 500 ps for analysis, at 3 cpu hours per picosecond), using the procedure described for the bilayer.
18. H. De Loof, S. C. Harvey, J. P. Segrest, R. W. Pastor, *Biochemistry* **30**, 2099 (1991).
19. R. W. Pastor, R. M. Venable, M. Karplus, A. Szabo, *J. Chem. Phys.* **89**, 1128 (1988).
20. D. F. Bocian and S. I. Chan, *Annu. Rev. Phys. Chem.* **29**, 307 (1978); E. Rommel, F. Noack, P. Meier, G. Kothe, *J. Phys. Chem.* **92**, 2981 (1988).
21. M. F. Brown, A. A. Ribeiro, G. D. Williams, *Proc. Natl. Acad. Sci. U.S.A.* **80**, 4325 (1983); M. F. Brown, *J. Chem. Phys.* **80**, 2808 (1984).
22. *Landolt-Bornstein Tables* (Springer-Verlag, Berlin, ed. 6, 1969), vol. II.5.
23. W. L. C. Vaz and P. F. Almeida, *Biophys. J.* **60**, 1553 (1991).
24. J. Tabony and B. Perly, *Biochim. Biophys. Acta* **1063**, 67 (1990).
25. R. M. Venable and R. W. Pastor, in preparation.
26. See (*10*), chap. 7.
27. T. M. Fischer, *Biophys. J.* **63**, 1328 (1992), and references therein.
28. We thank the Division of Computer Research and Technology at the National Institutes of Health for providing computer time on the IBM 3090; B. Brooks for technical advice as well as computer time; and A. MacKerell, M. Schlenkrick, J. Brickmann, and M. Karplus for providing a copy of PARM 22 before publication.

24 May 1993; accepted 3 August 1993

Dissipation of Marine Stratiform Clouds and Collapse of the Marine Boundary Layer Due to the Depletion of Cloud Condensation Nuclei by Clouds

Andrew S. Ackerman,* Owen B. Toon, Peter V. Hobbs

When the production of cloud condensation nuclei in the stratocumulus-topped marine boundary layer is low enough, droplet collisions can reduce concentrations of cloud droplet numbers to extremely low values. At low droplet concentrations a cloud layer can become so optically thin that cloud-top radiative cooling cannot drive vertical mixing. Under these conditions, model simulations indicate that the stratocumulus-topped marine boundary layer collapses to a shallow fog layer. Through this mechanism, marine stratiform clouds may limit their own lifetimes.

Marine stratiform clouds overlie about a third of the Earth's oceans and play a prominent role in the Earth's radiative heat balance (*1*). As shown by satellite imagery, marine stratiform clouds reflect much more sunlight than the darker underlying ocean surface and strongly enhance the Earth's global albedo (*2*). It has been estimated that the global cooling that would result from a 4% increase in the area covered by marine stratocumulus would offset the expected warming from a doubling of atmospheric carbon dioxide concentrations (*3*). Extensive sheets of marine stratocumulus are a climatological feature of the eastern regions of subtropical oceans, where the planetary boundary layer is capped by a strong temperature inversion produced by large-scale subsidence. The vertical mixing that supplies moisture to these clouds and maintains the depth of the boundary layer is generally driven by cloud-top radiative cooling (*4*). Clearly, an understanding of the processes that determine the lifetime and albedo of marine stratocumulus is of critical importance to an understanding of the Earth's climate system.

Twomey (*5*) suggested that increased numbers of cloud condensation nuclei (CCN) can enhance cloud albedo because they increase the droplet surface area for a fixed mass of cloud water. Albrecht (*6*) argued that increased CCN concentrations, which decrease cloud droplet sizes and reduce drizzle, can increase the fractional coverage of marine stratiform clouds because drizzle can regulate the liquid-water content and the lifetime of a cloud. Evidence that increases in particle concentrations can increase cloud albedo is provided by linear high-albedo cloud features over the ocean, often hundreds of kilometers long, known as "ship tracks" because they are caused by emissions from ships (*7, 8*). In this report we identify a phenomenon that is the converse of ship tracks. We have found, through numerical modeling studies, that clouds themselves may reduce particle concentrations to such an extent that the clouds dissipate and, as a consequence, the boundary layer collapses.

Variations in CCN concentrations can strongly affect cloud cover (Fig. 1). In the dark, nearly cloud-free region shown in Fig. 1, low ambient CCN concentrations were measured from aboard a ship (*8*). There were apparently not enough CCN in this dark region to maintain an optically thick cloud layer. However, a prominent cloud line (ST in Fig. 1) formed behind an underlying ship during the same period. Along this line, the injection of a large number of CCN apparently allowed a persistent cloud to form.

We suggest that drizzle in marine stratiform clouds can reduce CCN concentrations sufficiently to cause the stratocumulus-topped boundary layer to collapse to a shallow fog layer, in which cloud-top radiative cooling can no longer drive vertical mixing. A typical scenario (scenario 1) for such a collapse would be for CCN concentrations to build under cloud-free conditions. Then, when clouds form, CCN concentrations are depleted by collisions between cloud droplets that have formed on CCN and by the removal of cloud water in drizzle. The reduction in CCN concentrations can lead to the dissipation of the clouds and the collapse of the boundary layer.

We used a numerical model (*9*) to investigate this process. The production of CCN in the model was represented by a constant CCN source of 5×10^{-4} cm^{-3} s^{-1} throughout the depth of the boundary layer (*10*). The model domain was initially unsaturated and cloudless (*11*). The initial CCN concentration of 100 cm^{-3} corresponds to a constant production rate over about 2 days of cloud-free conditions in which no significant loss processes are active. Once the simulation was started, it took $\sim$1.5 hours for a cloud layer to form (Fig. 2).

A. S. Ackerman and P. V. Hobbs, Department of Atmospheric Sciences, University of Washington, Seattle, WA 98195.
O. B. Toon, Ames Research Center, National Aeronautics and Space Administration, Moffett Field, CA 94035.

*To whom correspondence should be addressed.